Journal of Inflammation Research

Dovepress
Taylor & Francis Group

Open Access Full Text Article

ORIGINAL RESEARCH

Mechanism Study of Yi-Qi-Dao-Zhi Formula in Improving Postoperative Ileus by Targeting the TLR4/NF-κB/MAPK Signaling Pathways

Jing Yu[1,*], Xuan Zhao[1,*], Liuchuang Zhang[1], Yanlin Chen[1], Tianle Zhang[1], Ye Wang[1], Chen Yi[1], Huafeng Pan[2], Haifeng Wang[2], Miaomiao Ge[2], Zhiwei Jiang[2], Gang Wang[2]

[1]Affiliated Hospital of Nanjing University of Chinese Medicine, Nanjing, Jiangsu, People's Republic of China; [2]Department of General Surgery, Jiangsu Province Hospital of Chinese Medicine, Affiliated Hospital of Nanjing University of Chinese Medicine, Nanjing, Jiangsu, People's Republic of China

*These authors contributed equally to this work

Correspondence: Gang Wang; Zhiwei Jiang, Email gwang82@163.com; surgery34@163.com

Purpose: Postoperative ileus (POI) commonly impedes recovery after surgical procedures. While the Yi-Qi-Dao-Zhi Formula (YQDZ) has proven its worth in treating premature ovarian insufficiency in clinical settings, the exact therapeutic mechanisms that make it tick continue to fly under the radar.

Methods: This investigation employed ultra-performance liquid chromatography combined with quadrupole time-of-flight mass spectrometry (UPLC-Q-TOF-MS/MS) to pinpoint the key bioactive compounds in YQDZ. For in vivo experiments, a POI mouse model was created through surgical intervention, and gastrointestinal transport function was assessed via charcoal ink experiments. Intestinal histopathology was examined using HE staining. The therapeutic impact of YQDZ on POI was thoroughly assessed using a battery of advanced laboratory techniques, including immunofluorescence staining, immunohistochemical analysis, Western blot procedures, real-time quantitative PCR assays, and ELISA testing. In vitro experiments involved the establishment of an M1-type inflammatory model by inducing mouse mononuclear macrophage RAW264.7 cells with LPS. Additional evaluations encompassed CCK-8 assays, flow cytometry, transcriptomic profiling, real-time PCR, and protein level examinations, all aimed at delving into the mode of action of YQDZ.

Results: YQDZ steers M1 macrophage differentiation through the TLR4/NF-κB/MAPK signaling pathway. This action effectively curtails the levels of key inflammatory mediators including TNF-α, IL-1β, and IL-6. Consequently, it acts as a therapeutic agent for inflamed bowels in postoperative ileus mice, helping to restore their gastrointestinal functionality.

Conclusion: The therapeutic approach of YQDZ for POI might be connected to the adjustment of the TLR4/NF-κB/MAPK signaling pathway, alongside the inhibition of macrophage polarization.

Keywords: Yi-Qi-Dao-Zhi Formula, postoperative ileus, macrophage, TLR4/NF-κB/MAPK signaling pathway

Introduction

Postoperative ileus (POI) is characterized by gastrointestinal motility dysfunction following abdominal surgery. Clinical manifestations include abdominal discomfort, bloating, queasiness, and emetic episodes. In severe instances, POI can result in oral feeding intolerance and difficulties with defecation due to the cessation of anal exhaust, thereby impacting postoperative recovery and patients' quality of life.[1] Furthermore, the duration of POI directly influences the length of hospital stays, subsequently affecting medical expenses. Research indicates that approximately 40% of patients in the United States who undergo open abdominal surgery experience a POI duration exceeding five days, with the total annual cost for POI prevention and treatment reaching as high as 750 million US dollars.[2] Consequently, investigating effective treatment strategies to reduce the duration of POI holds significant clinical importance.

https://doi.org/10.2147/JIR.S589449
Received: 22 December 2025
Accepted: 21 February 2026
Published: 28 February 2026

Graphical Abstract

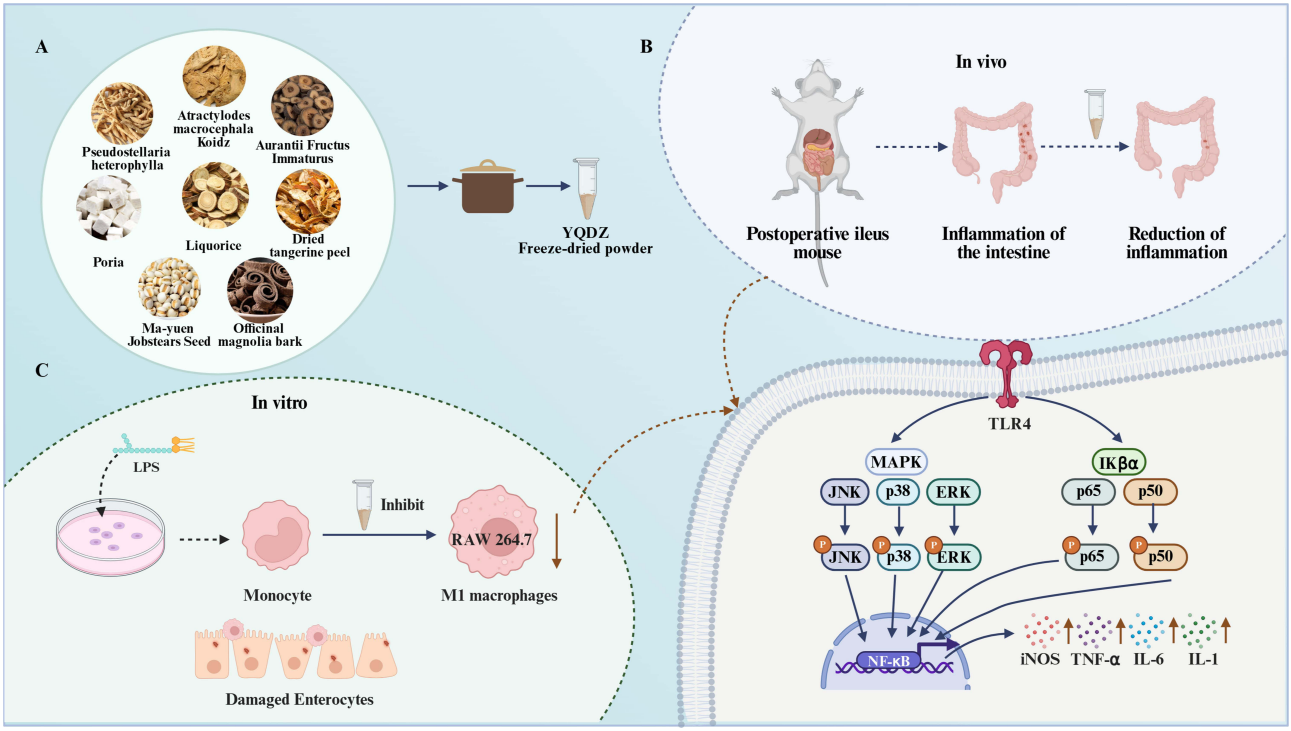

The mechanism underlying POI is intricate, encompassing various factors, including surgical trauma, inflammatory responses, neuroendocrine dysregulation, and pharmacological influences.[1] Notably, the local inflammatory response within the intestine serves as a central component in the onset and progression of POI, acting as a critical factor that contributes to the sustained impairment of intestinal motility following surgery.[3]

Surgical trauma can activate the innate immune system, which recognizes damp-associated molecular patterns (DAMPs) through Toll-like receptor 4 (TLR4) and initiates NF-κB and MAPK signaling pathways.[4–6] When TLR4 is activated, it sets in motion the myD88-dependent pathway, which subsequently stimulates the IKK complex. This sequence of events leads to the breakdown of IκBα, allowing p65 to break free and make its way to the nucleus where it sparks the transcriptional process for genes that promote inflammation. On the other hand, p38, ERK and JNK in the MAPK pathway are also activated, synergistically amplifying the inflammatory signal.[7–9] These two pathways push macrophages down the M1 polarization path, a process that triggers a vigorous production of pro-inflammatory cytokines such as TNF-α, IL-1β, and IL-6. This leads to the recruitment of immune cells like neutrophils, which sets off a inflammatory cascade. As a consequence, the smooth muscles in the intestines suffer from compromised contractile ability and motility issues.[10,11]

Macrophages significantly impact POI-triggered gut inflammatory responses.[12] Muscularis macrophages in the intermuscular nerve plexus of the intestinal wall are among the first to be activated following surgical trauma. They are not only the main amplifiers of inflammatory signals but also directly involved in regulating intestinal motility function.[7] Turned on macrophages churn out heaps of inflammatory agents and chemokines, luring neutrophils into the gut lining. This messes with local tissue swelling and spikes oxidative stress, ultimately making it tough for the gut to bounce back to its usual motion.[8] In addition, the inflammatory mediators secreted by macrophages can also affect the activity of the enteric nervous system, making intestinal peristalsis even more sluggish.[9] Therefore, inhibiting the excessive activation of macrophages can significantly alleviate local intestinal inflammation and promote postoperative intestinal motility recovery. In conclusion, macrophages may be a key target for the treatment of POI.

Current therapeutic options for POI are limited. Pharmacological interventions often yield suboptimal efficacy and carry considerable side effects.[13] For instance, prokinetic agents like metoclopramide show inconsistent outcomes, while NSAIDs are constrained by cardiovascular and gastrointestinal risks.[14] This therapeutic gap underscores the urgent need for safer alternatives. Traditional Chinese medicine, with its demonstrated benefits in functional gastrointestinal disorders, offers a promising approach for POI intervention.[15] The Yi-Qi-Dao-Zhi Formula (YQDZ) is an empirical formula for treating POI after gastric cancer surgery by Zhu Yongkang, a renowned traditional Chinese medicine doctor in Jiangsu Province.[16] It is derived from the Four Junzi Decoction and consists of ingredients such as *Pseudostellaria heterophylla* (Miq). Pax (Taizishen), *Atractylodes macrocephala* Koidz. (Baizhu), *Poria cocos* (Schw.) Wolf (Fuling), *Coix lacryma-jobi* L. (Yiyiren), *Citrus aurantium* L. (Zhishi), Magnolia officinalis Rehd. et Wils. (Houpo), Citrus reticulata Blanco (Chenpi), *Glycyrrhiza uralensis* Fisch. (Gancao). Detailed information on the herbal components and medicinal parts of YQDZ is shown in Table 1. Despite compelling clinical evidence demonstrating YQDZ's effectiveness in managing postoperative ileus symptoms and promoting restored gastrointestinal function, the precise molecular mechanisms underlying these therapeutic benefits continue to elude researchers.[17] Accordingly, this research will conduct a thorough investigation into the precise biological pathways through which YQDZ combats Premature Ovarian Insufficiency, utilizing both living organism and laboratory-based experiments. The objective is to establish a solid pharmacological foundation for the prescription's clinical implementation while further illuminating the scientific principles underlying the therapeutic approach of " Tonify Qi and relieve stagnation".

Materials and Methods

Reagents

p-ERK (#4370), ERK (#4695), p-p38 (#4511), p38 (#8690), p-p65 (#3033), p65 (#8242) were obtained from Cell Signaling Technology (CST) (MA,USA). p-JNK (T40074) and iNOS (T55993) were purchased from Abmart (Shanghai, China). TLR4 (66,350-1-Ig), JNK (24164-1-AP), GAPDH (60004-1-Ig), mouse secondary antibody (RGAM001), and rabbit secondary antibody (RGAR001) were purchased from Proteintech Group, Inc. (Wuhan, China). Inflammatory Factor Elisa kits IL-1β and TNF-α were purchased from Epizyme Biomedical Technology Co.,Ltd. (Shanghai, China). IL-6 was purchased from Elabscience Biotechnology Co.,Ltd. (Wuhan, China), and the fluorescent antibody FITC-CD86 was purchased from BD Biosciences (Shanghai, China).

Preparation of YQDZ

YQDZ utilized in this study was supplied by the Jiangsu Province Hospital of Chinese Medicine (Jiangsu, China). Detailed herb composition and medicinal parts of YQDZ appear in Table 1. Two lots of herbal substances (cumulatively 210 grams) underwent immersion in six cups of water for half an hour before being boiled for the same duration. After straining the mixture, the collected liquid was set aside for later experimentation. The remaining solids were then boiled once more with six times their volume of water for half an hour before being strained again. The two filtrates were merged and subjected to vacuum concentration at 75 °C. After concentration, 25 mL of the extract was precisely dispensed into each centrifuge tube. Prior to lyophilization, the samples were flash-frozen at –80 °C for a full day before

Table 1 Detailed Information of Herbs in YQDZ

Chinese Name	Latin Name	Medicinal Parts	Amount (g)
Taizishen	*Pseudostellaria heterophylla* (Miq.) Pax	Dried root	12
Baizhu	*Atractylodes macrocephala* Koidz.	Dried root	20
Fuling	*Poria cocos* (Schw.) Wolf	Dried root	15
Yiyiren	*Coix lacryma-jobi* L.	Dried Seed	20
Zhishi	*Citrus aurantium* L.	Dried fruit	12
Houpo	*Magnolia officinalis* Rehd. et Wils.	Dried root	10
Chenpi	*Citrus reticulata* Blanco	Dried fruit peel	6
Gancao	*Glycyrrhiza uralensis* Fisch.	Dried root	10

https://doi.org/10.2147/JIR.S589449

being processed with a FuruiJet intelligent lyophilizer (Venus4502T pro) under specific parameters of –90 °C and 37 Pa. The lyophilized YQDZ extract yielded approximately 28.5 g of powder from 210 g of raw herbs, corresponding to a yield of 13.6% (w/w). Based on this yield, the low dose (7.965 g/kg raw herb equivalent in mice) translates to approximately 1.08 g/kg of lyophilized extract. According to the body surface area conversion formula,[18] this mouse dose is equivalent to approximately 0.087 g/kg in humans, which is close to the standard clinical daily dose of the raw formula (approximately 0.13 g/kg raw herb equivalent for a 60 kg adult). The high dose (15.93 g/kg) represents approximately twice this clinical equivalent.

UPLC-Q-TOF-MS/MS Analysis of YQDZ

Portion out 50 milligrams of the lyophilized YQDZ Formula powder, pulverize it thoroughly, and combine with 500 microliters of the extraction solution featuring the isotope-labeled internal standard (prepared in a 2:2:1 methanol-to-acetonitrile-to-water volumetric ratio). Vortex the mixture to ensure thorough mixing, followed by homogenization and ultrasonication. This process should be repeated three times. After allowing the mixture to stand for 30 minutes, centrifuge for 15 minutes. Obtain the supernatant and incubate for 10 minutes prior to a second 15-minute centrifugation. Following filtration, the test solution is obtained. To isolate the desired compounds, we turned to a sophisticated Vanquish ultra-high-performance liquid chromatography system from Thermo Fisher Scientific, which was paired with a Phenomenex Kinetex C18 column (2.1 mm × 100 mm, 2.6 μm). The column was packed with a mobile phase that was a 1:1 (by volume) mix of isopropanol and acetonitrile, with a touch of 0.01% acetic acid. The sample was stored at a chilly 4°C, and only 2 microliters were injected into the system. As for the analytical side, we deployed a Q Exactive HFX mass spectrometer in the IDA mode to gather MS/MS spectra. The settings for the DDA method were dialed in like this: a sheath gas flow of 50 arb, an auxiliary gas flow of 15 arb, a capillary temperature of 320°C, full MS resolution at 60,000, MS/MS resolution at 15,000, and collision energies that ramped up from 20 to 40 in the sNCE mode. The spray voltages were +3.8 kV for positive ions and −3.4 kV for negative ones.

Cell Culture and Cell Viability Assay

The RAW 264.7 murine macrophage cell line, used in this study, was purchased from the Stem Cell Bank of the Chinese Academy of Sciences (Shanghai). The cells were cultured in a complete growth medium enriched with 10% fetal bovine serum and 100 U/mL penicillin–streptomycin solution. These cells were incubated at an optimal temperature of 37°C in a humidified atmosphere containing 5% carbon dioxide. To keep these cells thriving and in prime condition, they were subcultured every 2–3 days, which helped maintain their robust growth and health. Cell viability was assessed using the CCK-8 method. The cells were seeded in 96-well dishes with a cell count of 10,000 per well. Following a 12-hour incubation period, we introduced varying dosages of YQDZ (ranging from 0 to 400 micrograms per milliliter) into the wells. The experimental treatment was then maintained for another 12 hours. Next, the mixture with 10% CCK-8 was poured into each well and allowed to sit for an hour. Afterward, the absorbance was taken at a 450 nm wavelength.

Cell Grouping

RAW264.7 cells were resuspended and categorized into four groups: Control, LPS, YQDZ, and YQDZ treatment. The Control group comprised untreated normal cells, while the LPS group included cells cultured with LPS (1 μg/mL) for 24 hours. The YQDZ group comprised cells incubated with YQDZ at a concentration of 200 μg/mL over a 24-hour period. Meanwhile, the YQDZ treatment group underwent an initial LPS stimulation at 1 μg/mL for 6 hours, followed by an 18-hour exposure to YQDZ at the same 200 μg/mL dosage.

Flow Cytometry Analysis

To evaluate macrophage polarization, we employed flow cytometric analysis. All experimental cell populations underwent fixation at ambient temperature utilizing a 4% paraformaldehyde solution for a duration of 30 minutes, subsequently subjected to two rinses with phosphate-buffered saline (PBS). The cells were then permeabilized through exposure to 0.3% Triton X-100 for 5 minutes, followed by two additional PBS washes. Next, cell samples were blocked with 200 mL of 1% bovine serum albumin (BSA) for 1 hour to prevent non-specific binding. Following centrifugation to remove the

blocking solution, 0.25 μg of FITC-conjugated CD86 antibody was introduced to the cell pellet, with incubation at 40°C maintained for 30 minutes. The cells received two final PBS washes before being passed through a 40 μm mesh filter. Finally, cell polarity measurements were acquired using flow cytometry.

Transcriptome

RAW264.7 cells were categorized into three groups: Control, LPS, and YQDZ treatment cohorts. RNA extraction from the cells was performed using the TRIzol method. Following quality assessment, the samples were sent to Hangzhou Lianchuan Biotechnology Co., Ltd. for transcriptome sequencing. The sequencing was conducted on the Illumina NovaSeqTM 600 platform, employing the PE150 dual-end sequencing mode. The data processing workflow is as follows: First, the fastp software was utilized for quality control of the raw sequencing data. Subsequently, gene and transcript assembly was accomplished using StringTie software, with quantification expressed in FPKM values. To analyze the differential expression of genes, we turned to the edgeR package in R. We set the threshold for recognizing genes with altered expression at a P-value below 0.05 and a fold change of over 1.2, Specifically, $\log2(FC) > 1$ signified up-regulation, $\log2(FC) < -1$ signified down-regulation, while the rest were deemed non-significant. Once we'd identified the differentially expressed gene, we delved into functional enrichment using the KEGG database. We also churned out visual representations, such as PCA graphs, volcano plots, GSEA charts, and KEGG pathway enrichment factor graphs.

Animals and Models

Beijing Weitong Lihua Laboratory Animal Technology Co., Ltd. provided 25 male C57 mice aged 6 to 8 weeks, weighing between 20 and 22 grams. From the outset, all animals were housed in a pathogen-free facility with strictly controlled environmental conditions, maintaining a consistent 12-hour day/night cycle in a temperature-regulated setting. Throughout the experimental period, the mice were provided with free round-the-clock access to both food and water.

After a 7-day acclimatization phase, the rodents were arbitrarily divided into five separate groups, with 5 mice in each group: (1) Sham group (Sham), (2) POI group (POI), (3) YQDZ Low-dose group (YQDZ-L, 7.965 g/kg), (4) YQDZ High-dose group (YQDZ-H, 15.93 g/kg), (5) Mosapride group (MSBL, 2.28 mg/kg).

The preparation of the POI model in C57 mice has been documented in the literature.[19] In brief, mice fasted for 24 hours with water access, followed by isoflurane anesthesia. A 2 cm abdominal incision was made, and pre-moistened gauze was placed on either side. The small intestine was excised using sterilized ophthalmic forceps, then washed with normal saline for three cycles of four minutes each until congestion and edema were observed. The small intestine was then retracted sequentially. One hour following the completion of the modeling, the treatment group mice received the drug via gavage at the specified dose. In contrast, the control and model groups were administered an equivalent volume of normal saline at 10 mL/kg by gavage every 12 hours. Following the experiment, pentobarital sodium (60 mg/mL) was intraperitoneally injected at a dose of 0.067 to 0.083 mL, calculated based on the body weight of the mice (20 to 25 g). The mice's breathing stopped within one minute, and then cervical dislocation was performed to euthanize the mice. Then, the middle ileum tissue was fixed in 4% paraformaldehyde to facilitate histological examination and immunohistochemical analysis. The remaining sections were subsequently frozen at −80°C for future applications.

The sample size (n=5 per group) was determined based on prior experience with the POI mouse model. This approach also adheres to the 3Rs principles (Replacement, Reduction, Refinement) to minimize animal usage. All animal protocols had been cleared by the Ethics Committee of the Affiliated Hospital of Nanjing University of Chinese Medicine (2024DW-061-01).

Evaluation of the Intestinal Motility

To assess gastrointestinal motility function, a carbon ink propulsion test was performed 48 hours post-operation.[20] Specifically, mice received a 5% activated carbon suspension via gavage, dosed according to their body weight (0.1 mL/10 g). This particular mixture was prepared by combining 0.5 grams of activated carbon with 0.25 grams of gum Arabic, which were then thoroughly dissolved in 10 milliliters of normal saline solution. Following 15 minutes of intragastric administration, the mice were anesthetized and euthanized, allowing for the rapid isolation of the intact small intestines. The researchers took precise measurements of the charcoal and ink mixture's placement in the small intestine and the

entire length of the small intestine itself. They then computed the intestinal insertion rate by dividing the mixture's insertion length by the total length of the small intestine, and multiplying that figure by 100%.

Histomorphology

After being preserved in 4% polyoxymethylene fixative for a full day, the ileum samples underwent a standard processing protocol that included dehydration, paraffin infiltration, and embedding. The tissue slices were subsequently treated with hematoxylin and eosin (HE) in line with standard lab protocols, resulting in the production of HE-stained slides that were ready for examination. An inverted optical microscope visualized and documented the intestinal structure. Additionally, Slideviewer software was deployed to assess the dimensions of intestinal villi and the density of the mucosal base in each of the study's experimental groups.

Immunofluorescent Staining

After dewaxing and hydrating the paraffin sections, antigen retrieval was performed under high heat and pressure. The tissues were then blocked with 10% normal donkey serum for 30 minutes. Primary antibodies were applied and incubated overnight in a refrigerated environment at 4°C. The next day, we rinsed the sections three times with TBST buffer before applying the secondary antibody, which was then incubated at 37 °C away from light for 45 minutes. After washing, nuclei were stained with DAPI (1:500) and the sections were mounted with an anti-fade medium. Imaging was conducted using an Olympus BX53 fluorescence microscope and captured with the Pannoramic SCAN II system.

Immunohistochemistry Assay

Paraffin-embedded tissue sections were dewaxed, rehydrated, and subjected to antigen retrieval. Sections were then incubated with primary antibodies overnight at 4 °C, followed by secondary antibody incubation for 45 min at room temperature. Color development was performed using DAB, after which nuclei were counterstained with hematoxylin. Following dehydration and mounting, brown DAB-positive signals and blue nuclear staining were visualized microscopically. Images were acquired using an optical microscope, and semi-quantitative analysis of positive staining was conducted with ImageScope software.

Real-Time Polymerase Chain Reaction (RT-qPCR)

We harvested RNA from both RAW 264.7 cells and mouse ileal tissues employing the FastPure Cell/Tissue Total RNA Isolation Kit (Vazyme, Nanjing, China). This was then converted into complementary DNA through reverse transcription, after which we conducted real-time PCR to analyze the samples. We gauged the mRNA expression levels quantitatively through the 2 -ΔΔCT methodology, using GAPDH as our housekeeping gene for reference. The target genes along with their specific primers were custom-designed and synthesized by Shanghai Jierui Bioengineering Co., LTD. The sequences for all primers are detailed in Supplementary Table 1.

Western Blot Analysis

We assessed protein levels in both RAW264.7 cells and intestinal tissues using Western blotting. To determine protein concentration, we employed a BCA assay kit sourced from Epizyme in Shanghai. For the procedure, we loaded 20 μg of protein per well, separated them via SDS-PAGE electrophoresis, and then transferred the proteins to a PVDF membrane. After blocking the membrane with 5% BSA for one hour at room temperature, we applied the primary antibody and allowed it to incubate overnight. On the subsequent day, the membrane underwent three rinses with Tris-buffered saline solution supplemented with Tween-20, following which the secondary antibody was left to incubate at ambient temperature for a full hour. Following another round of three washes, visualization was performed using a chemiluminescent gel imaging system, specifically the Tanon chemiluminescence detection platform. Subsequent analysis of the resulting gel images was carried out with ImageJ software.

Statistical Analysis

All data are presented as mean ± standard deviation. Statistical analyses were performed using GraphPad Prism 9 software. To compare differences between groups, we conducted a one-way analysis of variance (ANOVA). A P-value less than 0.05 was considered statistically significant, whereas a P-value below 0.01 indicated high statistical significance.

Results

UPLC-Q-TOF-MS/MS Analysis of YQDZ

The quality of YQDZ was assessed using UPLC-Q-TOF-MS/MS technology, which facilitated the identification of its compounds. In the positive ion scanning mode, a total of 27 distinct chemicals were pinpointed, as depicted in Figure 1A, with comprehensive details available in Supplementary Table 2. The chromatogram for negative ion mode is presented in Figure 1B, revealing 22 identified chemical components; further details can be found in Supplementary Table 3. The results show that flavonoids and saponins constitute the major bioactive components of YQDZ, implying that its anti-inflammatory activity may arise from the combined effects of multiple constituents.

YQDZ Improves Intestinal Inflammation in POI Mice

To assess the therapeutic efficacy of YQDZ on POI, we developed a POI model via surgical intervention. Initially, we evaluated the gastrointestinal peristaltic function using a carbon-ink experiment. Results revealed that the intestinal transit rate in POI model mice was markedly reduced when compared to the Sham group, pointing to a significant impairment in gut transport capabilities (Figure 2B). Furthermore, YQDZ treatment effectively restored gastrointestinal peristalsis in a dose-dependent manner, with the high-dose group demonstrating an improvement comparable to that of the prokinetic agent mosapride (Figure 2A). Subsequently, histopathological assessment was conducted to evaluate morphological changes in the ileal tissue. In the POI group, we observed marked mucosal edema, villous destruction, and extensive infiltration of inflammatory cells in the intestine (Figure 2C). Following YQDZ treatment, the damage to the ileal tissue in mice was significantly mitigated, as evidenced by a reduction in inflammatory cell infiltration and an enhancement in the integrity of the mucosal structure (Figure 2D and E). In order to bolster the evidence of YQDZ's anti-inflammatory effects, we employed real-time quantitative PCR and ELISA techniques to measure the concentrations of key inflammatory cytokines, including TNF-α, IL-1β, and IL-6, in samples of intestinal tissue. Our data clearly indicated that the POI model group displayed significantly heightened concentrations of these pro-inflammatory markers, whereas YQDZ administration strikingly diminished their expression in a dose-dependent manner (Figure 2F–J). The above results fully demonstrate that YQDZ can effectively improve intestinal motility disorders in POI and alleviate intestinal inflammation.

YQDZ Inhibits the Infiltration of Macrophages in the Intestinal Tissue of POI Mice

Macrophages play a crucial role in inflammation following POI. To investigate the impact of YQDZ on the infiltration of intestinal macrophages, we employed immunofluorescence staining for detection. The staining results indicated that the ileal tissue structure in the Sham group remained intact, with a weak background signal. Compared with the control, the POI group showed intense F4/80 signals in the ileal region, suggesting predominant macrophage accumulation within the mucosal and submucosal compartments. This finding suggests considerable inflammatory infiltration induced by surgical stress. Following treatment with YQDZ, the F4/80 signal was markedly diminished, and both the number and distribution of macrophages were significantly reduced. The high-dose treatment group showed a striking inhibitory effect that stood shoulder to shoulder with the results achieved by the positive control medication, mosapride (Figure 3). Therefore, we conclude that YQDZ effectively mitigates the abnormal infiltration of macrophages induced by POI.

YQDZ Inhibits M1 Polarization and Inflammation of RAW264.7 Macrophages Induced by LPS

To evaluate YQDZ's direct impact on macrophage polarization, we established an M1 inflammatory model using LPS-induced RAW264.7 cells. Initially, we turned to the CCK-8 test to assess how YQDZ affected the survival rate of the RAW264.7 cells. The results indicated that YQDZ promoted cell proliferation at concentrations below 200 μg/mL, while

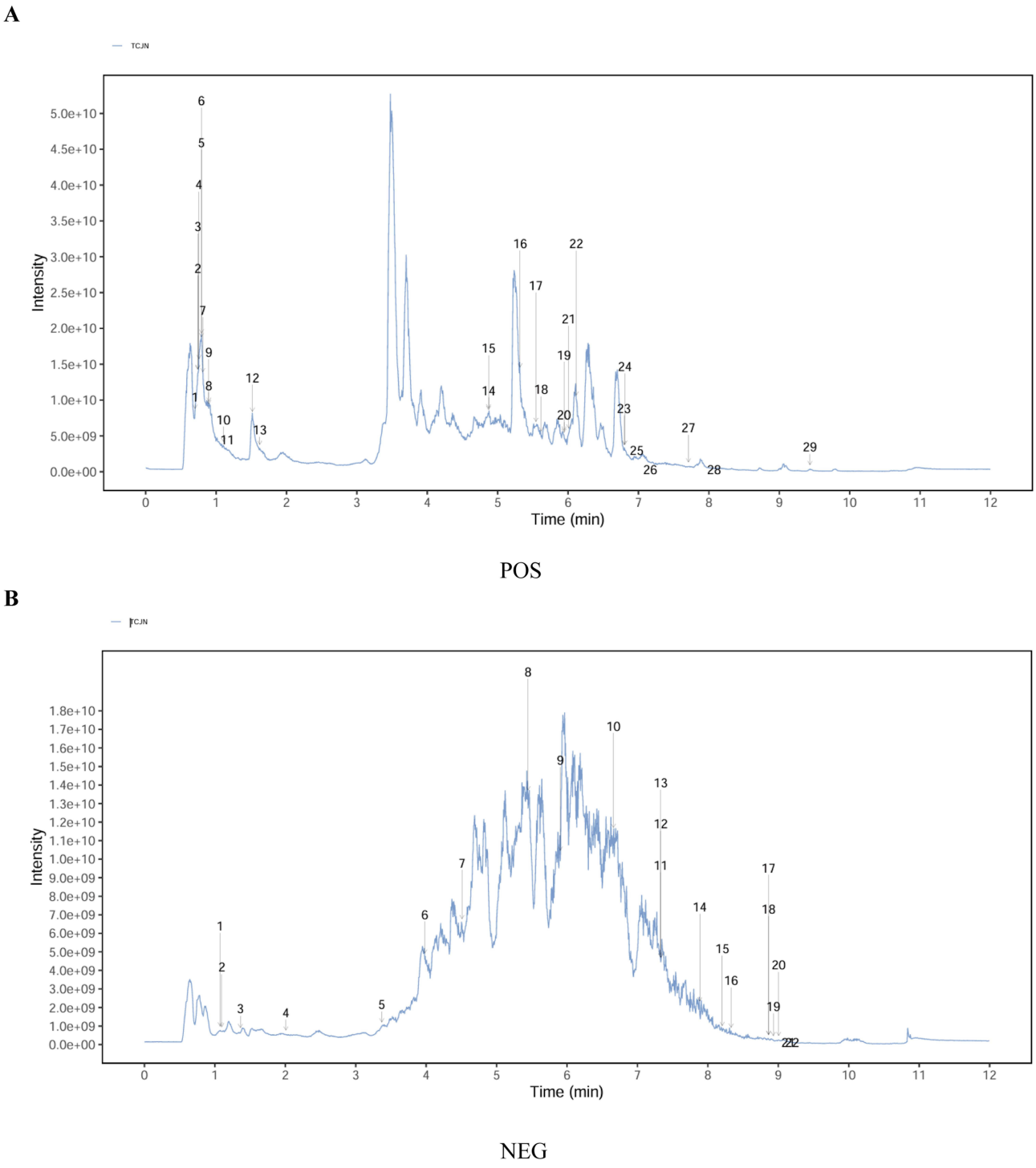

Figure 1 The UPLC-Q-TOF-MS/MS total ion chromatograms (TICs) of the YQDZ extract are presented in positive ion mode (**A**) and negative ion mode (**B**).

exhibiting a significant dose-dependent inhibitory effect at concentrations exceeding this threshold. Thus, 200 μg/mL was identified as the ideal dosage for further testing (Figure 4A). The data from the flow cytometry analysis showed a dramatic shift in macrophages towards the M1 profile upon LPS stimulation, a trend marked by a bump in the percentage of CD86 expressing cells. However, this pattern reversed with the application of YQDZ, as indicated by the stark decrease in CD86 expression levels (Figure 4B). What's more, YQDZ had a substantial effect on curbing the release of IL-6 and TNF-α in the cell culture fluid (Figure 4C and D) and down-regulated the mRNA expression levels of IL-1β

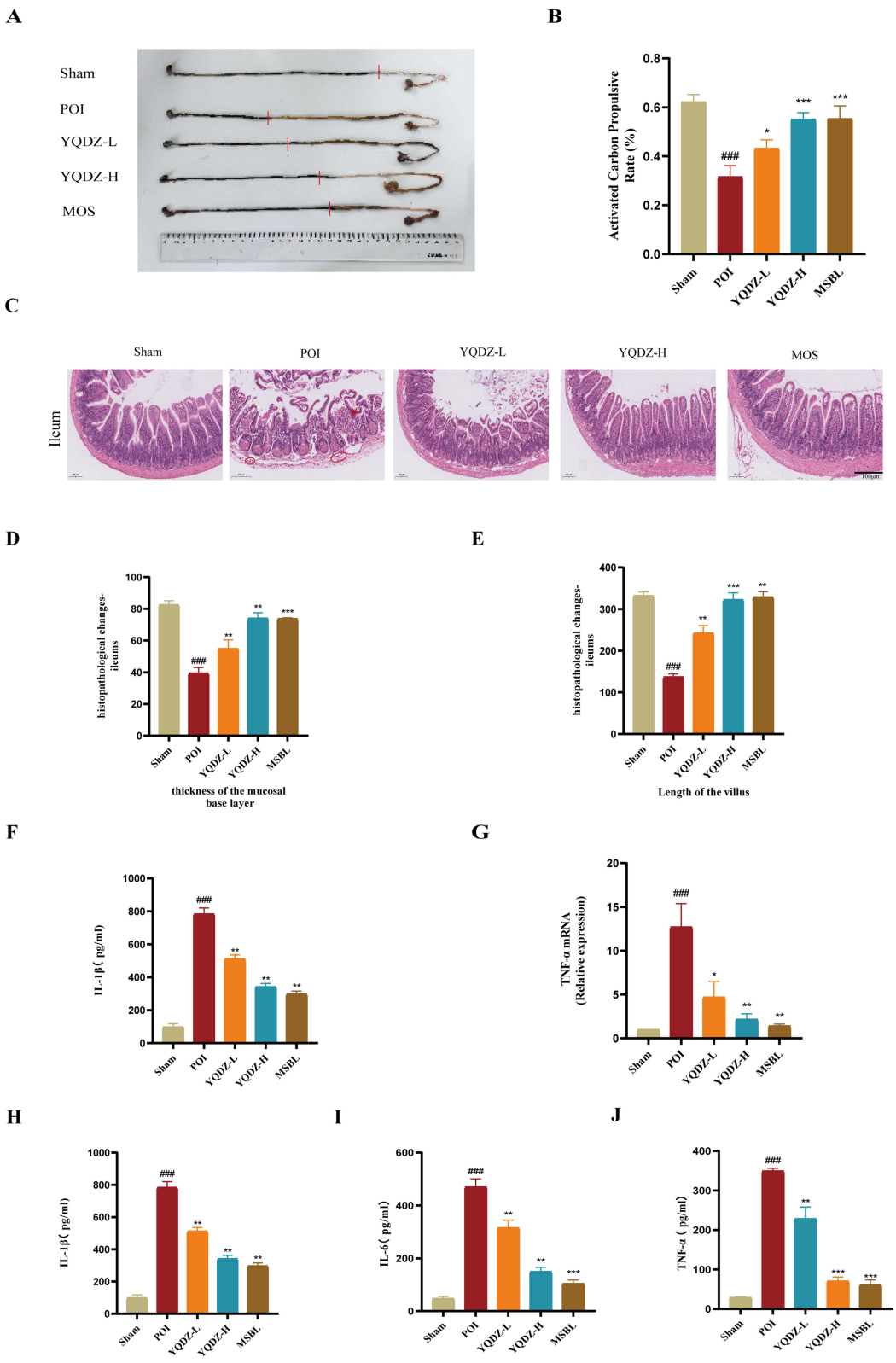

Figure 2 YQDZ improves intestinal peristalsis ability and alleviates ileal inflammation in the POI mouse model. (**A**) Representative images of activated carbon propulsion in each group (Sham, POI, YQDZ-L, YQDZ-H and MSBL) (n=3). (**B**) Quantitative results of the activated carbon advancement rate (n=3). (**C**) Representative H&E staining sections of ileal tissues in each group (scale = 100μm, n=3). Histological quantification of the thickness of the mucosal basal layer and the length of villi (**D** and **E**) (n=3). (**F** and **G**) The mRNA expression levels of IL-1β and TNF-α in ileal tissue were determined by RT-qPCR (n=3). (**H–J**) The expression levels of IL-1β, IL-6 and TNF-α in ileal tissue were determined by ELISA (n=3). All data are reported as mean ± SD, and significance testing was conducted using one-way ANOVA. Compared with the Control group, $^{###}P < 0.001$; compared with the POI group, $^{*}P < 0.05$, $^{**}P < 0.01$. $^{***}P < 0.001$.

https://doi.org/10.2147/JIR.S589449

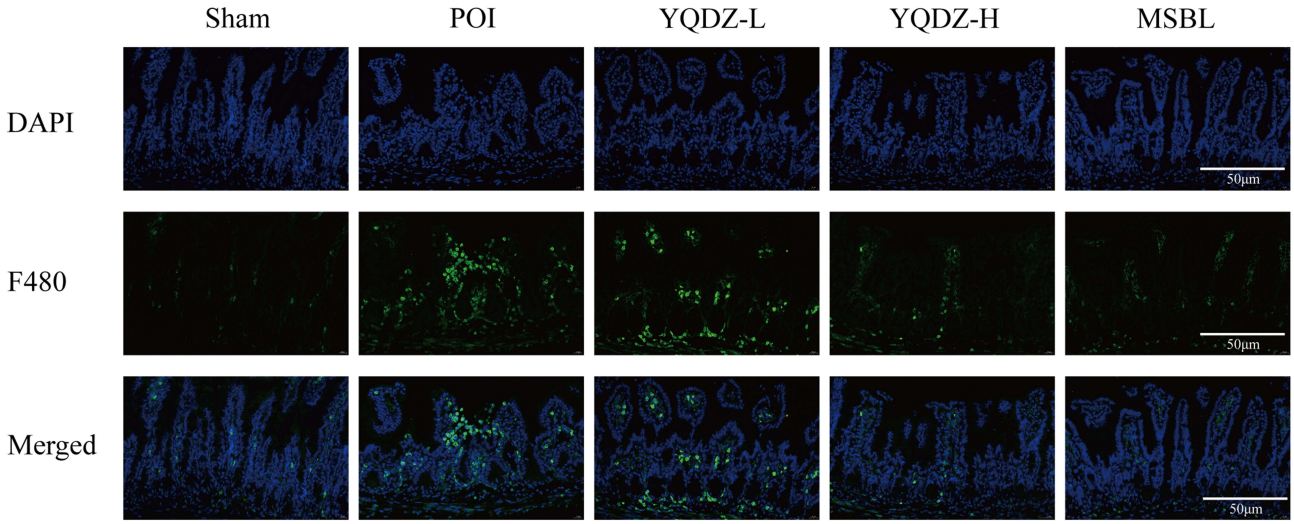

Figure 3 Shows the representative images of immunofluorescence staining. The ileum sections were stained with DAPI (blue) and F480 (green), and observed under a fluorescence microscope (scale = 50 μm, n=3).

and TNF-α (Figure 4E–G), indicating its efficacy in suppressing LPS-induced inflammatory responses. Thus, this study suggests that YQDZ can directly target macrophages, reducing inflammation through blocking M1 transformation and pro-inflammatory mediator synthesis.

Transcriptomic Analysis of LPS-Induced Mouse Macrophages

In order to delve deeper into the mode of operation of YQDZ, RNA sequencing was conducted on the RAW264.7 cells from the control, LPS, and YQDZ treatment cohorts. A thorough analysis of differentially expressed genes highlighted a striking contrast between the LPS cohort and the YQDZ-treated group, pinpointing 7,109 genes that varied in expression. Among these, 4,118 genes were upregulated, while 2,991 experienced a downregulation (Figure 5A). Furthermore, an extensive examination across the LPS and Control groups uncovered a total of 9,302 genes displaying differential expression. This included 4,188 genes that were upregulated and 5,132 genes that were downregulated (Figure 5B). Principal component analysis demonstrated significant overall differences among the three sample groups (Figure 5C). The KEGG pathway analysis revealed a notable enrichment of the genes that showed differential expression within the Toll-like receptor pathway, and also within the MAPK and NF-κB signaling pathways (Figure 5D). Furthermore, the GSEA outcomes pointed to the potential of YQDZ intervention to potently quash the activation of these pathways, including Toll-like receptors, MAPK, and NF-κB (Figure 5E–G). The results clearly demonstrate that YQDZ has the ability to put the brakes on LPS-triggered inflammatory pathway activation, paving the way for future mechanistic investigations.

YQDZ Suppresses the Initiation of the TLR4/NF-κB/MAPK Pathway in Macrophages Triggered by LPS

To corroborate our transcriptomic results, we set up in vitro tests to examine the expression of iNOS, a pivotal indicator of M1 macrophages, alongside proteins implicated in the TLR4/NF-κB/MAPK signaling cascade. Western blotting showed LPS markedly increased JNK, p38, and ERK phosphorylation in RAW264.7 cells. Additionally, it markedly upregulated the expression of iNOS and TLR4 while concurrently activating downstream NF-κB, as evidenced by a significant increase in p-p65 levels (Figure 6). Treatment with YQDZ significantly reversed these alterations. These findings align with the transcriptomic analysis, further demonstrating that YQDZ can inhibit LPS-induced M1 polarization and the inflammatory response in macrophages by suppressing the activation of the TLR4/NF-κB/MAPK signaling pathway.

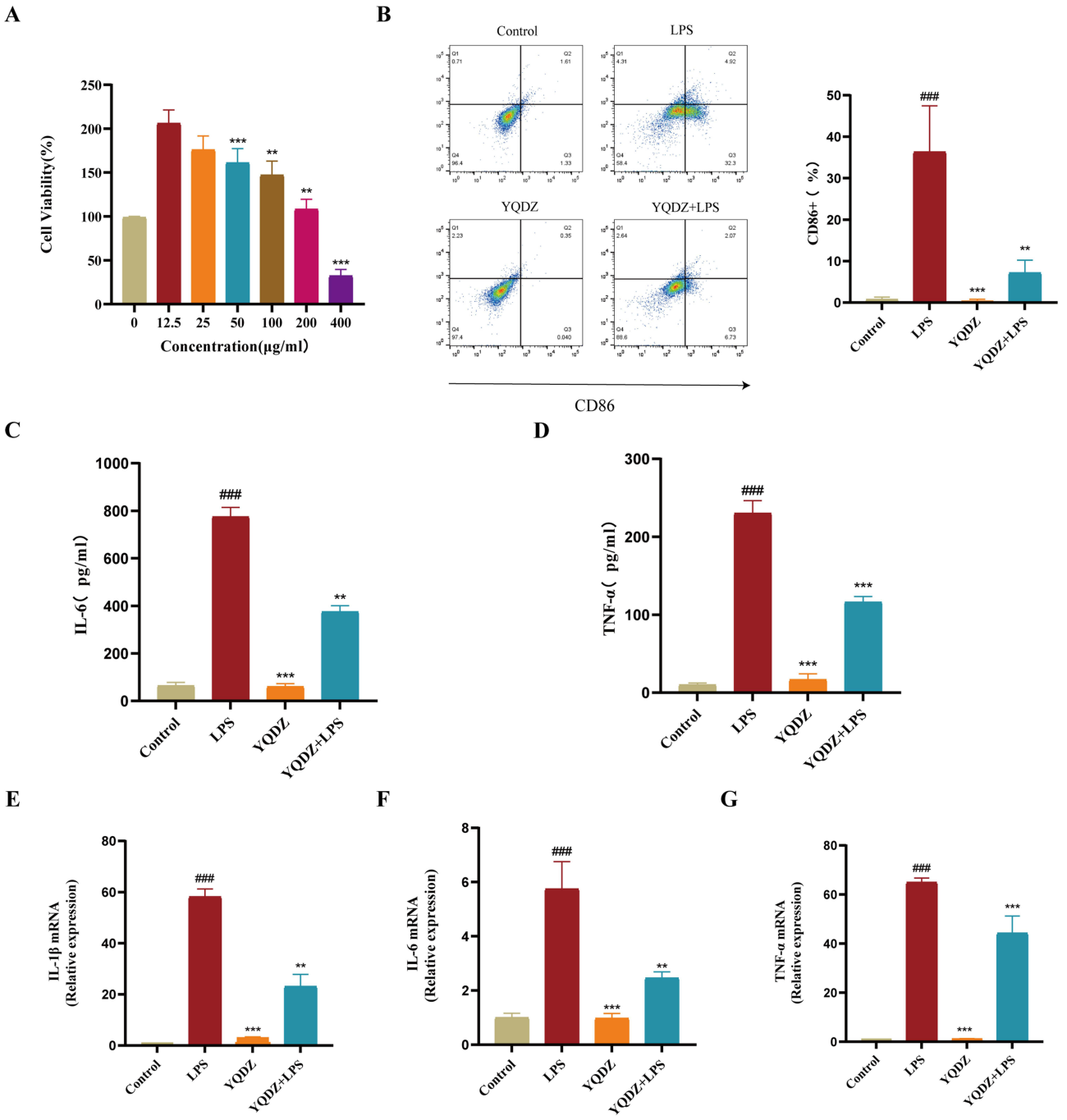

Figure 4 YQDZ alleviates LPS-induced inflammatory activation and M1 polarization of RAW264.7 macrophages. (**A**) The viability of RAW264.7 macrophages exposed to various concentrations of YQDZ for 24 hours was assessed using the CCK-8 assay (n = 3). (**B**) Flow cytometry was used to analyze the expression of CD86, reflecting the polarization degree of M1 (n=3). (**C** and **D**) ELISA analysis showed the secretion levels of IL-6 and TNF-α in the supernatants of the Control group, LPS group, YQDZ group and YQDZ+LPS group (n=3). (**E**–**G**) The mRNA expression levels of IL-1β, IL-6 and TNF-α in each group were detected by RT-qPCR (n=3). All data are reported as mean ± SD, and significance testing was conducted using one-way ANOVA. Compared with the Control group, $^{###}P < 0.001$; compared with the LPS group, $^{**}P < 0.01$. $^{***}P < 0.001$.

YQDZ Improves Intestinal Inflammation in POI Mice by Inhibiting the TLR4/MAPK/NF-κB Pathway

In vitro findings show YQDZ's capacity to suppress LPS-stimulated macrophage inflammation and trigger the TLR4/MAPK/NF-κB cascade. To get a clearer picture of its anti-inflammatory effects in mice, we took a closer look at protein expression within the TLR4/NF-κB/MAPK pathway in the ileal tissue of mice with postoperative ileus. The immunohistochemical investigation disclosed that YQDZ suppressed the levels of phosphorylated proteins, including TLR4, p-p65, p-p38, and

https://doi.org/10.2147/JIR.S589449

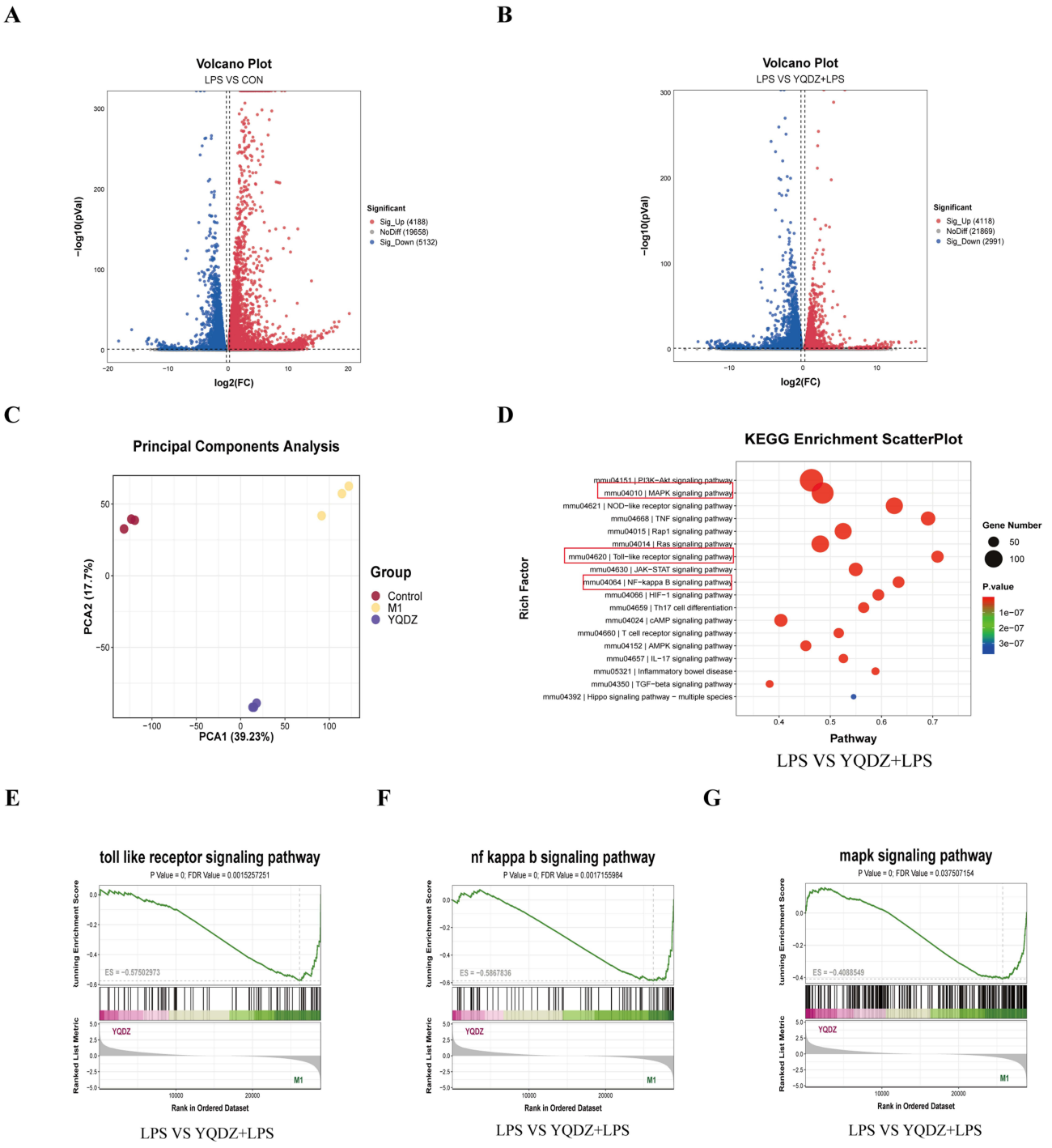

Figure 5 Transcriptome analysis demonstrated that YQDZ can reverse LPS-induced inflammatory transcriptional activation in RAW264.7 macrophages. (**A**) Volcano plots illustrate the differentially expressed genes between the LPS group and the CON group. (**B**) Volcano plots depict the differentially expressed genes between the LPS group and the YQDZ treatment group. (**C**) PCA plots represent the gene expression profiles in each group. (**D**) The KEGG pathway map highlights the differentially expressed genes. GSEA plots of the Toll-like receptor, NF-κB and MAPK signaling pathways are presented between the (**E–G**) LPS group and the YQDZ treatment group.

p-ERK, in a manner that correlated with the dose used in the study, both in vitro and within the living organism (Figure 7). We delved deeper into the manifestation of these proteins through a Western blot examination, and the findings aligned perfectly with the outcomes from the immunohistochemical test (Figure 8). Taken together, these discoveries indicate that YQDZ is a real player in throttling the over-the-top activation of the TLR4/NF-κB/MAPK pathway caused by POI, which makes it a key player in anti-inflammatory and tissue-saving measures.

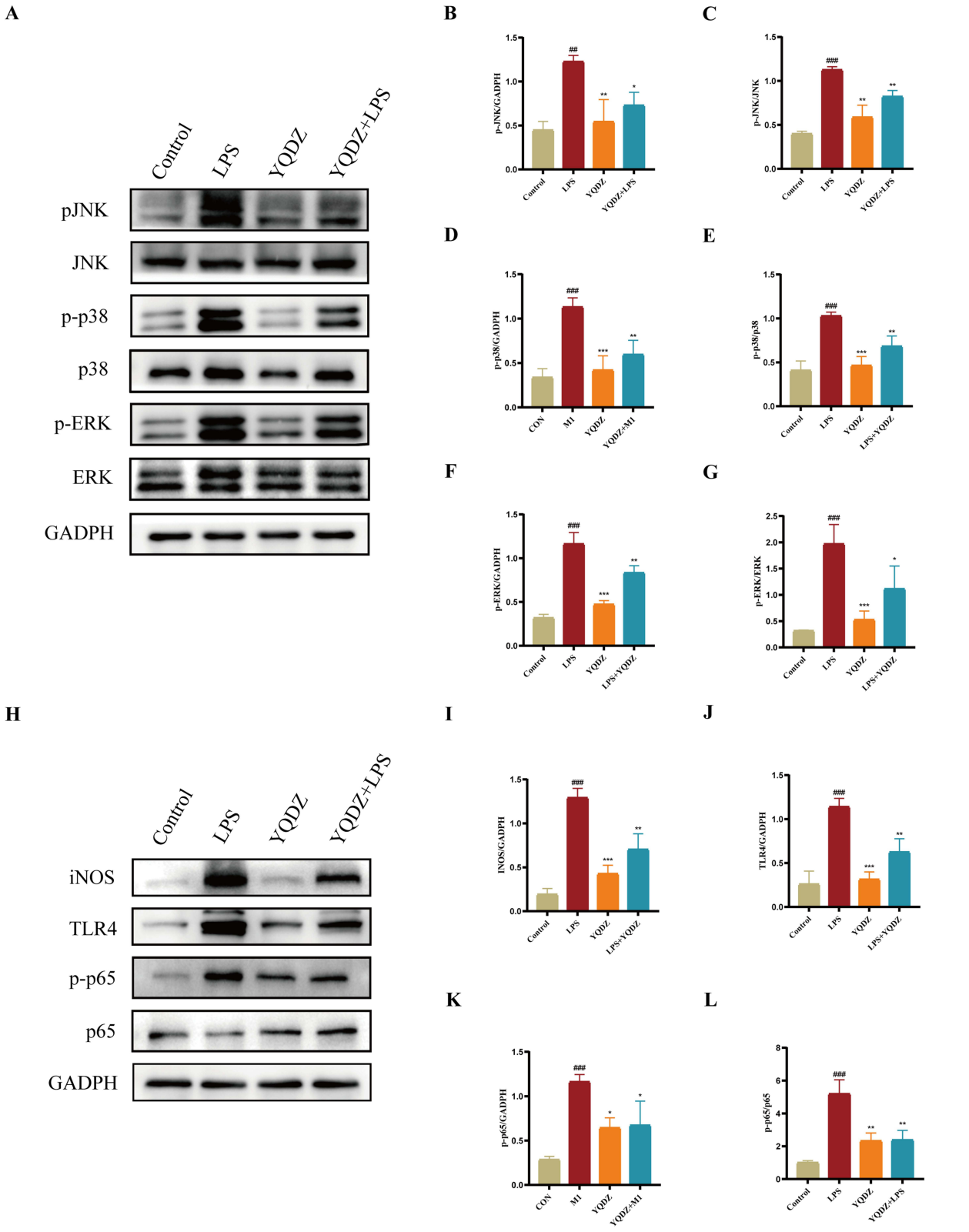

Figure 6 YQDZ inhibits the activation of the TLR4/NF-κB/MAPK signaling pathway in LPS-stimulated RAW264.7 macrophages. (**A**) The protein bands of p-JNK, JNK, p-p38, p38, p-ERK, ERK and GAPDH in each group were detected by Western blot (n=3). Relative protein quantification of (**B**–**G**) p-JNK, p-p38 and p-ERK. (**H**) Western blot was used to detect the protein bands of iNOS, TLR4, p-p65, p65 and GAPDH in each group (n=3). (**I**–**L**) Relative protein quantification of iNOS, TLR4 and p-p65 (n=3). All data are reported as mean ± SD, and significance testing was conducted using one-way ANOVA. Compared with the Control group, ####P < 0.001; compared with the LPS group, *P <0.05, **P < 0.01. ***P < 0.001.

https://doi.org/10.2147/JIR.S589449

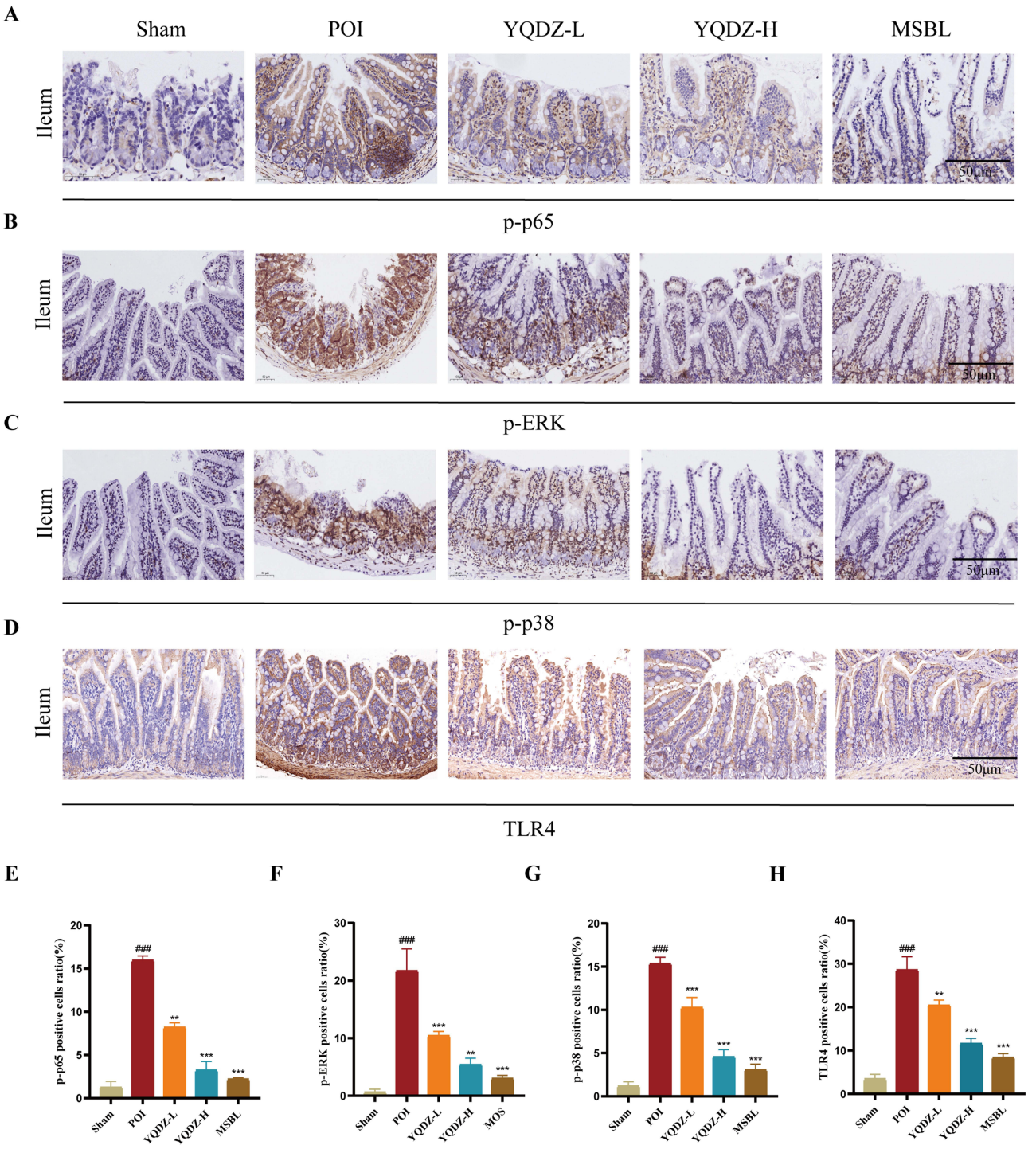

Figure 7 Effects of YQDZ on the TLR4/NF-κB/MAPK signaling pathway in ileal tissue of mice. (**A**–**D**) Immunohistochemical methods for detecting the expressions of p-p65, p-ERK, p-p38, and TLR4 in ileal tissue (scale =50μm, n=3), (**E**–**H**) p-p65, p-ERK Quantitative analysis of p-p38, TLR4 (n=3). All data are reported as mean ± SD, and significance testing was conducted using one-way ANOVA. Compared with the Control group, $^{###}P < 0.001$; compared with the POI group, $^{**}P < 0.01$. $^{***}P < 0.001$.

Discussion

POI is initiated by surgical trauma, leading to a transient phase of neurosuppression, which subsequently develops into a localized intestinal inflammatory response characterized by innate immune activation. This process ultimately results in persistent gastrointestinal motility disorders. As a significant factor influencing postoperative recovery, current treatment strategies for POI require enhancement in clinical efficacy.[21,22] YQDZ, a traditional Chinese medicine compound used

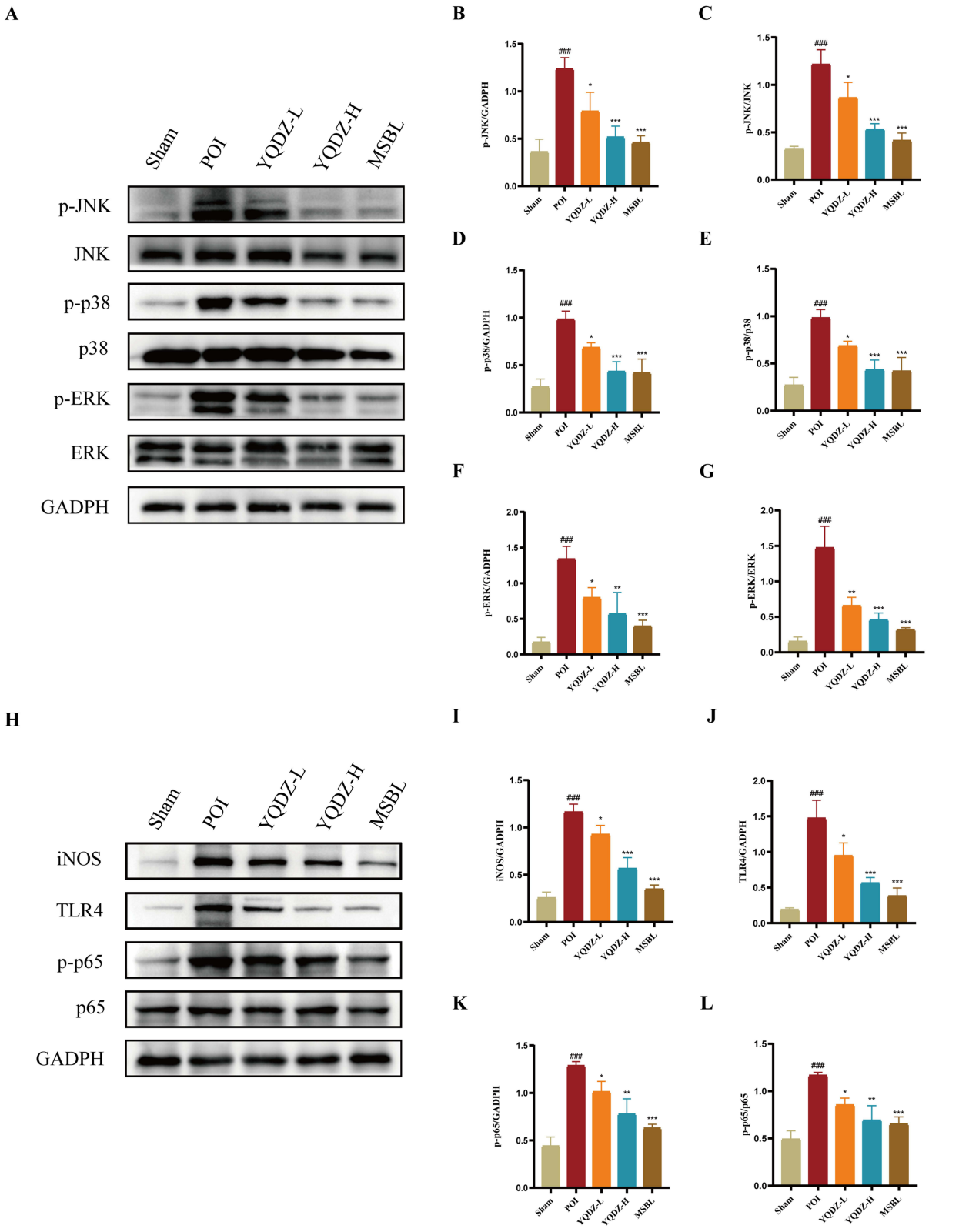

Figure 8 YQDZ inhibits the activation of the TLR4/NF-κB/MAPK signaling pathway in POI mice. (**A**) The protein bands of p-JNK, JNK, p-p38, p38, p-ERK, ERK and GAPDH in each group were detected by Western blot (n=3). Relative protein quantification of (**B**–**G**) p-JNK, p-p38, and p-ERK (n=3). (**H**) The protein bands of iNOS, TLR4, p-p65, p65 and GAPDH in each group were detected by Western blot (n=3). (**I**–**L**) Relative protein quantification of iNOS, TLR4 and p-p65 (n=3). All data are reported as mean ± SD, and significance testing was conducted using one-way ANOVA. Compared with the Control group, $^{\#\#\#\#}P < 0.001$; compared with the POI group, *P <0.05, **P < 0.01. ***P < 0.001.

https://doi.org/10.2147/JIR.S589449

for treating POI, has shown clinical effectiveness in several studies;[16,23] Nonetheless, the precise process of its functioning remains unclear. For the first time, our research reveals through comprehensive in vivo and in vitro investigations that YQDZ successfully curbs macrophage polarization while dampening inflammatory reactions by fine-tuning the TLR4/NF-κB/MAPK signaling cascade, ultimately slowing down the harmful advancement of POI.

YQDZ consists of various traditional Chinese medicines and encompasses multiple components, including flavonoids, saponins, and phenolic compounds. The synergistic interactions among these components can enhance the anti-inflammatory properties of YQDZ. Previous studies have demonstrated that flavonoids and phenolic compounds pack a punch when it comes to antioxidant power, enabling them to directly tackle free radicals and reactive oxygen species head-on. Consequently, oxidative stress–induced neuronal damage is attenuated, inflammatory signal transduction is suppressed, and the levels of pro-inflammatory cytokines are reduced.[24–26] Furthermore, saponin compounds demonstrate anti-inflammatory effects through several mechanisms. They effectively regulate cytokines and chemokines, subsequently diminishing immune cell migration towards inflammatory regions.[27,28]

Inflammation critically impacts postoperative ileus (POI) development and course, with macrophages serving as the primary infiltrating white blood cells during the initial inflammatory response.[29,30] Following surgical trauma or intestinal manipulation, muscularis macrophages are activated and secrete pro-inflammatory cytokines that recruit neutrophils, resulting in damage to intestinal tissues and mucosal inflammation, which ultimately contribute to the development of POI.[31,32] In animal models of POI, intestinal myolayer macrophages have been identified as the "initiating cell population" responsible for postoperative aseptic inflammation and gastrointestinal motility disorders. Inhibition or depletion of these macrophages can significantly reduce intestinal inflammation and enhance gastrointestinal peristalsis.[32,33] This demonstrates that local myometrial macrophages are central to the pathogenic mechanisms underlying POI. In our experimental study, we noted a significant reduction in the secretion of key inflammatory markers—such as IL-1β, IL-6, and TNF-α—within the ileal tissue of mice with POI, thanks to the effects of YQDZ. Moreover, YQDZ spurred an increase in intestinal motility. The compound also managed to dampen the activity of the pro-inflammatory protein iNOS, effectively cushioning the impact on the intestinal lining and its villi. Laboratory tests revealed that YQDZ potently blocked LPS from prompting macrophage polarization and the discharge of these inflammatory agents. These insights hint that YQDZ has the potential to ease POI symptoms by mitigating the inflammation triggered by the M1 polarization of macrophages.

Studies have demonstrated that macrophage function relies on the stimulation of membrane receptors and the intricate regulation of various intracellular factors. Together, these molecular cues drive macrophages to shift from a quiescent to an active phenotype, consequently modifying their function within the body's defense mechanisms.[34] Furthermore, macrophage activation encompasses not only a singular immune response but also includes polarization processes, such as the differentiation into M1-type and M2-type macrophages.[35] These distinct polarization states influence the varying response patterns of macrophages during inflammation, infection, and tissue repair. In summary, macrophage activation is a highly complex and meticulously regulated process that involves multiple signaling pathways and cascade reactions. Consequently, further investigation into the molecular mechanisms by which YQDZ inhibits macrophage polarization and treats POI is of considerable importance.

Within the intricate web of signaling pathways that control macrophage activation, the TLR4/NF-κB/MAPK axis plays a pivotal role in orchestrating inflammatory reactions. Studies show that the immune system's reaction to surgery is a major factor in the onset of postoperative ileus. Post-injury, locally released DAMPs are picked up by TLR4, triggering the innate immune system into action. As a key pattern recognition receptor, TLR4 identifies not only signals from external pathogens but also internal injury signals, subsequently setting off a cascade of immune responses.[36] The activation of TLR4 predominantly occurs through the MyD88-dependent pathway, which initiates the activation of the IKK complex. This activation subsequently engages the NF-κB pathway, leading to an increased expression of pro-inflammatory factors and, as a result, exacerbating inflammation.[37,38] When NF-κB goes into overdrive, it can trigger chronic inflammation that further exacerbates intestinal harm and disrupts digestive tract movement.[39,40] In the context of postoperative ileus, NF-κB activation walks hand in hand with heightened inflammatory gene expression in the intestinal mucosa, effectively throwing a spanner in the works of normal gastrointestinal function. The findings of this study show

that inflammatory stimulation markedly elevates TLR4 and iNOS expression in RAW264.7 cells and in the ileal samples from POI mice, whereas YQDZ treatment substantially reduces their levels.

It is worth noting that NF - κB is not an isolated pathway but highly interacts with pathways such as MAPK, jointly regulating immune responses and the emission of inflammatory agents. The MAPK crew includes p38, ERK, and JNK, and they are key in managing cellular stress reactions, cell growth, differentiation, and cell death.[41] Studies suggest that in a multitude of inflammatory and tissue-damage related ailments, a persistent go at the MAPK signaling route can light up the production of pro-inflammatory cytokines and escalate the activation of immune cells, thereby cranking up the inflammatory response. Over-activating this pathway is closely linked to the breakdown of the intestinal mucosal barrier and the exacerbation of intestinal harm.[42] Conversely, the overall inhibition of the MAPK pathway contributes to the down-regulation of inflammatory mediators, including TNF-α, IL-1β, and IL-6. This inhibition reduces inflammatory cell infiltration and histopathological damage, thereby exerting anti-inflammatory and mucosal protective effects.[43] Transcriptomic analyses revealed significant activation of the Toll-like receptors, MAPK, and NF-κB signaling pathways. Notably, YQDZ treatment markedly inhibited this activation. Moreover, findings from the immunohistochemistry and Western blot analyses showed a considerable upregulation of proteins linked to the TLR4/NF-κB/MAPK signaling cascade in the model cohort, and the activation of this pathway was significantly inhibited after YQDZ intervention.

To wrap things up, this research demonstrates that YQDZ orchestrates the TLR4/NF-κB/MAPK signaling pathway, thereby curbing macrophage polarization and tamping down gut inflammation, which ultimately helps alleviate the symptoms of POI. However, several limitations should be noted. First, genetic knockout models or specific inhibitors are needed to confirm the causal role of this pathway. Second, the specific bioactive compounds in YQDZ responsible for its effects require further identification. Third, our animal model does not fully replicate the complexity of human patients with comorbidities and multimodal care. Therefore, these findings should be translated with caution, and the efficacy of YQDZ for POI requires validation in future clinical trials.

Conclusion

This study comprehensively details YQDZ's inflammation-reducing properties and its molecular pathways for improving POI. These effects are partially attributed to the inhibition of M1 macrophage polarization through modulation of the TLR4/NF-κB/MAPK signaling pathway. Our findings provide a mechanistic rationale for the clinical application of YQDZ in postoperative gastrointestinal dysfunction and highlight the multi-target therapeutic characteristics of traditional Chinese medicine formulas. As this is a preclinical study, the efficacy and safety of YQDZ require further confirmation in well-designed clinical trials.

ARRIVE Guidelines Statement

All animal experimental procedures strictly adhered to the ARRIVE guidelines. The mice were administered an excess of pentobarbital sodium via intraperitoneal injection at a concentration of 60 mg/mL, with the total volume ranging from 0.067 to 0.083 mL, based on their weight, which was between 20 to 25 grams. After at least one minute of cessation of breathing, the mice were subjected to cervical dislocation to confirm that they had passed away.

Data Sharing Statement

All data generated or analysed during this study are included in this published article and its supplementary information files.

Ethics Statement

All animal experiments were conducted strictly following the established protocols and ethical standards governing animal welfare at the Centre for Laboratory Animal Care, Nanjing University of Chinese Medicine.

Acknowledgments

This work was supported by the Jiangsu Provincial Key Discipline Project (ZDXK202251), Jiangsu Provincial Association of Chinese Medicine Revitalization and Development Project (ZXFZ2024001), and Jiangsu Postgraduate Research Innovation Program (KYCX25_2279).

Author Contributions

Jing Yu (First Author) and Xuan Zhao (Co-first Author): Conceptualization, Data Curation, Formal Analysis, Investigation, Methodology, Software, Visualization, Writing-Original Draft, Writing-Review & Editing; Gang Wang and Zhiwei Jiang (Corresponding Author): Conceptualization, Funding Acquisition, Resources, Supervision, Validation, Writing-Original Draft, Writing-Review & Editing; Yanlin Chen: Methodology, Supervision; Writing-Review & Editing. Liuchuang Zhang: Supervision, Validation; Writing-Review & Editing. Tianle Zhang: Data Curation, Supervision; Writing-Review & Editing. Ye Wang: Investigation, Data Curation; Writing-Review & Editing. Chen Yi: Investigation, Data Curation; Writing-Review & Editing. Huafeng Pan: Supervision; Validation; Writing-Review & Editing. Haifeng Wang: Resources; Validation; Writing-Review & Editing. Miaomiao Ge: Investigation; Supervision; Writing-Review & Editing.

All authors gave final approval of the version to be published; have agreed on the journal to which the article has been submitted; and agree to be accountable for all aspects of the work.

Disclosure

No potential competing interest was reported by the authors.

References

1. Buscail E, Deraison C. Postoperative ileus: a pharmacological perspective. *Br J Pharmacol*. 2022;179(13):3283–3305. doi:10.1111/bph.15800
2. Venara A, Neunlist M, Slim K, et al. Postoperative ileus: pathophysiology, incidence, and prevention. *J Visc Surg*. 2016;153(6):439–446. doi:10.1016/j.jviscsurg.2016.08.010
3. Story SK, Chamberlain RS. A comprehensive review of evidence-based strategies to prevent and treat postoperative ileus. *Dig Surg*. 2009;26 (4):265–275. doi:10.1159/000227765
4. Relja B, Land WG. Damage-associated molecular patterns in trauma. *Eur J Trauma Emerg Surg*. 2020;46(4):751–775. doi:10.1007/s00068-019-01235-w
5. Ma M, Jiang W, Zhou R. DAMPs and DAMP-sensing receptors in inflammation and diseases. *Immunity*. 2024;57(4):752–771. doi:10.1016/j.i. mmuni.2024.03.002
6. Sun W, Hang L, Chen L, et al. Fraxin ameliorates ulcerative colitis by modulating oxidative stress, inflammation and TLR4/NF-κB and MAPK signaling pathways. *Altern Ther Health Med*. 2024;30(12):117–125.
7. Zhou L, Lian H, Yin Y, et al. New insights into muscularis macrophages in the gut: from their origin to therapeutic targeting. *Immunol Res*. 2023;71 (6):785–799. doi:10.1007/s12026-023-09397-x
8. Tsuchida Y, Hatao F, Fujisawa M, et al. Neuronal stimulation with 5-hydroxytryptamine 4 receptor induces anti-inflammatory actions via α7nACh receptors on muscularis macrophages associated with postoperative ileus. *Gut*. 2011;5:638–647. doi:10.1136/gut.2010.227546
9. Choi EL, Taheri N, Zhang Y, Matsumoto K, Hayashi Y. The critical role of muscularis macrophages in modulating the enteric nervoussystem function and gastrointestinal motility. *J Smooth Muscle Res*. 2024;60:1–9. doi:10.1540/jsmr.60.1
10. De Jonge WJ, van den Wijngaard RM, The FO, et al. Postoperative ileus is maintained by intestinal immune infiltrates that activate inhibitory neural pathways in mice. *Gastroenterology*. 2003;125(4):1137–1147. doi:10.1016/s0016-5085(03)01197-1
11. Schwarz NT, Kalff JC, Turler A, et al. Prostanoid production via COX-2 as a causative mechanism of rodent postoperative ileus. *Gastroenterology*. 2001;121(6):1354–1371. doi:10.1053/gast.2001.29605
12. Wehner S, Behrendt FF, Lyutenski BN, et al. Inhibition of macrophage function prevents intestinal inflammation and postoperative ileus in rodents. *Gut*. 2007;56(2):176–185. doi:10.1136/gut.2005.089615
13. Iskander O. An outline of the management and prevention of postoperative ileus: a review. *Medicine*. 2024;103(24):e38177. doi:10.1097/ MD.0000000000038177
14. Ulasi IB, Afuwape OO, Ayandipo OO, Fakoya A, Irabor DO. The effects of combined gum-chewing and parenteral metoclopramide on the duration of postoperative ileus after abdominal surgery. *J West Afr Coll Surg*. 2023;13(4):46–57. doi:10.4103/jwas.jwas_38_23
15. Liu R, Luo Y, Ma J, et al. Traditional Chinese medicine for functional gastrointestinal disorders and inflammatory bowel disease: narrative review of the evidence and potential mechanisms involving the brain-gut axis. *Front Pharmacol*. 2024; 15:1444922. doi:10.3389/fphar.2024.1444922
16. Hong Z, Yongkang Z. Zhu Yongkang's experience in the treatment of gastrointestinal dysfunction after surgical abdominal surgery using the "spleen movement method". *Jiangsu J Tradit Chin Med*. 2024;56(3):23–25. doi:10.19844/j.cnki.1672-397X.2024.03.006
17. Haiou N, Yuling C, Pengyan X, et al. Yiqi Daozhi formula promotes gastrointestinal function recovery after gastric cancer surgery:a randomized controlled trial. *Chin J Integrat Tradit Chin West Med*. 2020;45(1):25–31. doi:10.7661/j.cjim.20241217.166
18. Nair AB, Jacob S. A simple practice guide for dose conversion between animals and human. *J Basic Clin Pharm*. 2016;7(2):27–31. doi:10.4103/ 0976-0105.177703
19. Tian D, Liu B, Huang S, et al. Postoperative ileus murine model. *J Vis Exp*. 2024;10(209):3791/66465. doi:10.3791/66465
20. Morais TC, Arruda BR, de Sousa Magalhaes H, et al. Mangiferin ameliorates the intestinal inflammatory response and the impaired gastrointestinal motility in mouse model of postoperative ileus. *Naunyn Schmiedebergs Arch Pharmacol*. 2015;388(5):531–538. doi:10.1007/s00210-015-1095-4
21. Wang Z, Stakenborg N, Boeckxstaens G. Postoperative ileus-immune mechanisms and potential therapeutic interventions. *Neurogastroenterol Motil*. 2025;37(8):e14951. doi:10.1111/nmo.14951
22. Luckey A, Livingston E, Tache Y. Mechanisms and treatment of postoperative eus. *Arch Surg*. 2003;138(2):206–214. doi:10.1001/ archsurg1382.206
23. Pengyan X, Yuling C, Haiou N, et al. Based on heart rate variability, the effect of Yiqi conduction formula on the recovery of bowel function after colorectal cancer surgery was observed. *J Modern Integrat Med*. 2025;34(07):916–919+924.

24. Nani A, Murtaza B, Sayed Khan A, Khan NA, Hichami A. Antioxidant and anti-inflammatory potential of polyphenols contained in mediterranean diet in obesity: molecular mechanisms. *Molecules*. 2021;26(4):985. doi:10.3390/molecules26040985
25. l-Khayri JM, Sahana GR, Nagella P, Joseph BV, Alessa FM, Al-Mssallem MQ. Flavonoids as potential anti-inflammatory molecules: a review. *Molecules*. 2022;27(9):2901. doi:10.3390/molecules27092901
26. Jomova K, Alomar SY, Valko R, et al. Flavonoids and their role in oxidative stress, inflammation, and human diseases. *Chem Biol Interact*. 2025;413:111489. doi:10.1016/j.cbi.2025.111489
27. Wijesekara T, Luo J, Xu B. Critical review on anti-inflammation effects of saponins and their molecular mechanisms. *Phytother Res*. 2024;38 (4):2007–2022. doi:10.1002/ptr.8164
28. Dong J, Liang W, Wang T, et al. Saponins regulate intestinal inflammation in colon cancer and IBD. *Pharmacol Res*. 2019;144:66–72.
29. Liu T, Xu M, Shi Z, et al. Shenhuang plaster ameliorates the Inflammation of postoperative ileus through inhibiting PI3K/Akt/NF-κB pathway. *Biomed Pharmacother*. 2022;156:113922. doi:10.1016/j.biopha.2022.113922
30. Mao N, Yu Y, Lu X, Yang Y, Liu Z, Wang D. Preventive effects of matrine on LPS-induced inflammation in RAW 264.7 cells and intestinal damage in mice through the TLR4/NF-κB/MAPK pathway. *Int Immunopharmacol*. 2024;143(Pt 2):113432. doi:10.1016/j.intimp.2024.113432
31. Maehara T, Matsumoto K, Horiguchi K, et al. Therapeutic action of 5-HT3 receptor antagonists targeting peritoneal macrophages in post-operative ileus. *Br J Pharmacol*. 2015;172(4):1136–1147. doi:10.1111/bph.13006
32. Sui C, Tao L, Bai C, et al. Molecular and cellular mechanisms underlying postoperative paralytic ileus by various immune cell types. *Front Pharmacol*. 2022:If29901. doi:10.3389/fphar.2022.929901
33. Mallesh S, Schneider R, Schneiker B, et al. Sympathetic denervation alters the inflammatory response of resident muscularis macrophages upon surgical trauma and ameliorates postoperative ileus in mice. *Int J Mol Sci*. 2021;22(13):6872. doi:10.3390/ijms22136872
34. Choudhuri S, Chowdhury IH, Garg NJ. Mitochondrial regulation of macrophage response against pathogens. *Front Immunol*. 2021;11:622602. doi:10.3389/fimmu.2020.622602
35. Yunna C, Mengru H, Lei W, Weidong C. Macrophage M1/M2 polarization. *Eur J Pharmacol*. 2020;877:173090. doi:10.1016/j.jphar.2020.173090
36. Lim KH, Staudt LM. Toll-like receptor signaling. *Cold Spring Harb Perspect Biol*. 2013;5(1):a011247. doi:10.1101/cshperspecta011247
37. Wei J, Zhang Y, Li H, Wang F, Yao S. Toll-like receptor 4: a potential therapeutic target for multiple human diseases. *Biomed Pharmacother*. 2023;166:115338. doi:10.1016/j.biopha.2023.115338
38. Tang J, Xu L, Zeng Y, Gong F. Effect of gut microbiota on LPS-induced acute lung injury by regulating the TLR4/NF-kB signaling pathway. *Int Immunopharmacol*. 2021;91:107272. doi:10.1016/j.intimp.2020.107272
39. Atreya I, Atreya R, Neurath MF. NF-kappaB in inflammatory bowel disease. *J Intern Med*. 2008;263(6):591–596. doi:10.1111/j.1365-2796.2008.01953.x
40. Andresen L, Jørgensen VL, Perner A, Hansen A, Eugen-Olsen J, Rask-Madsen J. Activation of nuclear factor kappaB in colonic mucosa from patients with collagenous and ulcerative colitis. *Gut*. 2005;54(4):503–509. doi:10.1136/gut.2003.034165
41. Guo YJ, Pan WW, Liu SB, Shen ZF, Xu Y, Hu LL. ERK/MAPK signalling pathway and tumorigenesis. *Exp Ther Med*. 2020;19(3):1997–2007. doi:10.3892/etm.2020.8454
42. Chen D, Xiong Y, Lin Y. Dual role of MAPK pathway in the regulation of intestinal barrier function. *Inflamm Bowel Dis*. 2014;(7):20E16. doi:10.1097/MIB.0000000000000064
43. Yang S, Li W, Bai X, et al. Ginseng-derived nanoparticles alleviate inflammatory bowel disease via the TLR4/MAPK and p62/Nrf2/Keap1 pathways. *J Nanobiotechnology*. 2024;22(1):48. doi:10.1186/s12951-024-02313-x